The Co- and Immediate Post-seismic geodetic signature of the 1999 Hector Mine Earthquake

Kenneth J. Hurst†, Don Argus†, Andrea Donnellan†, Michael B. Heflin†, David Jefferson†, Gregory A. Lyzenga‡, Jay W. Parker†, Frank H. Webb†, James F. Zumberge†

† *Jet Propulsion Laboratory / California Institute of Technology*

‡ *Harvey Mudd College, and Jet Propulsion Laboratory / California Institute of Technology*

Introduction

The M7.1 Hector Mine earthquake ruptured the Lavic Lake fault near Twentynine Palms, CA at 09:46 UTC October 16, 1999. Because it occurred near the eastern edge of the Southern California Integrated GPS Network (SCIGN), a network of permanent, continuously recording GPS receivers for measuring the crustal deformation field around Los Angeles, CA, it was possible to determine the deformation associated with the earthquake with unprecedented speed and reliability. Thirty-four stations recorded displacements over the 3-sigma level. The displacements measured with GPS can be modeled by a fault 46.2 ± 2.6 km long, 8.2 ± 1.0 km wide, with 301 ± 36 cm right lateral strike-slip, and 145 ± 36 cm of east-up dip slip, yielding a potency of 1.3 km^3 and geodetic moment of 3.8×10^{26} dyne-cm. The trace and dip of the model fault is consistent with the observed ground rupture and seismic focal mechanisms.

Displacements measured with SCIGN data

The horizontal displacements in the International Terrestrial Reference Frame 1997 (ITRF97) [Boucher 1999] from the analysis of data from SCIGN done at the Jet Propulsion Laboratory (JPL) using the GIPSY software [Webb and Zumberge, 1995] are shown in Figure 1. They are derived from 4 days of GPS data prior to the earthquake (Oct 12-15) compared to 5 days of data after the earthquake (Oct 17-21). All days had the phase ambiguities resolved. Random walk zenith tropospheric delays, and tropospheric gradients as well as whitenoise receiver clocks were estimated at each station. Free-network precise GPS satellite orbits and clocks from the JPL global IGS analysis were used in the analysis [Zumberge et al 1997].

In postprocessing, the stations ALAM, DYER, ECHO, FERN, FRED, PVEP, SNI1, SPMX, and VNDP were used to define a local realization of the ITRF97 reference frame. PVEP is 220 km from the epicenter, and all the other reference stations are 350-450 km distant. At this distance the displacement should be negligible. After the solutions were aligned to a global definition of ITRF97 each of these stations was examined for anomalous behavior, and none was found. Finally, all 9 of the daily solutions were aligned to a local ITRF97 defined by a 9 day weighted average of these stations.

The 20 stations with displacements having a signal-to-noise ratio of 10 or larger are given in Table 1. The formal errors in the table (average over all stations = 1.0 mm N, 1.4 mm E, 4.3 mm V) are consistent with the daily repeatability before and after the quake. The χ^2/ν for the final combination was 0.86. A complete table of all station locations and displacements as well as time series of station positions are available from http://milhouse.jpl.nasa.gov/hector.

A kinematic analysis of the October 16 data from the station with the largest displacement, LDES, shows that the station moved approximately 17 cm during the main shock and 1 cm during a ML=5.6 aftershock about 13 minutes later. The position on subsequent days is indistinguishable from the position after this aftershock, indicating that any subsequent post-seismic motion at this station must be less than 2-3 mm in five days.

Inversion of GPS data

We present two inversions of the 3D station displacements described above for a single best-fit fault in an elastic half-space. In the first inversion, 8 parameters describing the fault (location, length, strike, dip, width, strike-slip, and dip-slip) were estimated. In the second inversion, the dip and dip-slip were constrained to 90 degrees and 0.0 cm respectively. For faults which break the surface, the inversion routine has difficulty estimating the uncertainty in the depth to the top of the fault. Since ground rupture has been identified in the field, [K. Hudnut, pers comm] and since preliminary inversions yielded depth=0.0 km, we held the depth fixed at 0.0 km in both inversions presented here. The values and uncertainties of the estimated parameters are given in Table 2.

In performing the inversions, we found that if the dip is estimated, the χ^2/ν drops by about 25%. If the dip is estimated, then the dip-slip must also be estimated or the resulting dip (53° west) is inconsistent with the seismic focal mechanism. When both dip and dip-slip are estimated, the dip is 85° to the east, consistent with the seismic focal mechanism. However, the resulting dip slip is 145 cm (east up) forming a rake angle of 154° compared with the Berkeley focal mechanism rake of 175° [http://www.seismo.berkeley.edu/seismo/eqw/99.10.16_mt.html] or the Harvard CMT focal mechanism rake of 179° [http://www.seismology.harvard.edu/CMTsearch.html]

The fact that the uncertainties needed to be scaled by 2 in the 8 parameter inversion and by 2.4 in the 6 parameter inversion to make $\chi^2/\nu = 1.0$ suggests that either the model is too simplistic or we have underestimated the errors in the GPS analysis. We prefer the former explanation since the formal errors of the GPS analysis are consistent with the daily repeatability. That the model should be too simplistic is hardly surprising since we have allowed only one fault in an elastic half-space and because at least some of the stations have probably experienced some post-seismic motion as discussed above.

The uncertainty parameters given in Table 2 are derived from examining the curvature of the cost function with respect to each parameter at the best fit location. Another reasonable assessment of the uncertainties in the fault parameter inversion would be to look at the difference between the two inversions presented here.

There is almost no information from SCIGN about deformation to the east of the quake because it occurred on the eastern edge of the partially completed network. The closest operating station, LDES, is still about 50 km (more than 1 fault length) away from the rupture. Because of this lack of azimuthal and near-field information, we confined our inversions to a single fault model. With additional data from campaign style measurements, and interferometric synthetic aperture radar, it will be possible to generate more detailed inversions.

The displacement field calculated from the 6 parameter inversion presented here was used in an elastic half-space screw dislocation model to generate a map of predicted displacements throughout the region as shown in the map in Figure 2a. In Figure 2b, the results of this forward model were then resolved onto the look angle for the ERS-2 radar satellite, and contoured to produce a prediction of the interferogram which should be derived from the ERS-2 radar data. We present this figure to help educate the intuition of the reader concerning which details of the radar interferograms being produced can be explained by a simple single crack in a half-space, and which details require other explanations.

Conclusion

The presence of the partially completed Southern California Integrated GPS Network (SCIGN) has allowed us to determine the co-seismic displacements from a M=7.1 earthquake with 1 mm horizontal precision and 3.5 mm vertical precision. Inversion of the displacements measured with GPS indicates that the earthquake can be modeled by a 46.2 ± 2.6 km long fault 8.2 ± 1.0 km wide, which slipped 301 ± 36 cm right lateral strike-slip, and 145 ± 36 cm of east-up dip slip.

Acknowledgements

First we would like to thank the other participants in the construction and operation of SCIGN, without which these results and this paper would not have been possible. These participants include colleagues from Scripps Institution of Oceanography, the United States Geological Survey, the University of California Los Angeles, and the University of Southern California. Funding for the construction and operation of

SCIGN comes from NASA, NSF, USGS, and the W. M. Keck foundation. The International GPS Service provides an essential service in coordinating the global network of tracking stations upon which the precise GPS orbits necessary for this study are founded.

References

Boucher, C., Z. Altamimi, and P. Sillard, The 1997 International Terrestrial Reference Frame (ITRF97), *IERS Tech. Note 27,* Obs de Paris, Paris, May 1999.

Webb, F. and J. Zumberge, An Introduction to GIPSY/OASIS II *JPL internal document D-11088* 1995.

Zumberge, J., M. Heflin, D. Jefferson, M. Watkins, and F. Webb, Precise point positioning for the efficient and robust analysis of GPS data from large networks, *J. Geophys. Res.,* 5005-5017, 1997.

http://milhouse.jpl.nasa.gov

http://www.seismology.harvard.edu/CMTsearch.html

http://www.seismo.berkeley.edu/seismo/eqw/99.10.16_mt.html

http://www-socal.wr.usgs.gov/hector

Figure Captions

1 Map of the measured displacements between October 12-15 and 17-21 1999, using data from the Southern California Integrated GPS Network. The data are the arrows with error ellipses at the end. The error ellipses are 95% confidence limits. The arrows without error ellipses are the displacements from a forward model using an elastic half-space and the fault parameters from the 8 parameter inversion discussed in the text. Green lines represnt faults. The heavy green line near the center of the map shows the trace of the rupture from this inversion.

2a The horizontal displacements from a forward model using an elastic half-space and the fault parameters from the 6 parameter inversion discussed in the text.

2b The 3D displacement field of the fault parameters from the 6 parameter inversion mapped into the direction to the ERS-2 satellite. The contour interval is 1 cm.

TABLE 1

Stations with displacements greater than 10 sigma

Station	Lat,Lon=Deg; Rad=m			m		m
LDES	LAT	34.2673	N	0.1791	±	0.0007
LDES	LON	-116.4328	E	0.0588	±	0.0008
LDES	RAD	978.0159	V	0.0178	±	0.0027
CTMS	LAT	34.1241	N	0.1043	±	0.0007
CTMS	LON	-116.3704	E	0.0328	±	0.0008
CTMS	RAD	966.4461	V	0.0132	±	0.0028
WIDC	LAT	33.9348	N	0.0528	±	0.0007
WIDC	LON	-116.3918	E	0.0171	±	0.0008
WIDC	RAD	445.0012	V	0.0079	±	0.0028
BSRY	LAT	34.9186	N	0.0154	±	0.0007
BSRY	LON	-117.0120	E	-0.0344	±	0.0007
BSRY	RAD	613.5068	V	-0.0094	±	0.0027
PSAP	LAT	33.8192	N	0.0321	±	0.0007
PSAP	LON	-116.4940	E	0.0114	±	0.0008
PSAP	RAD	86.7336	V	0.0060	±	0.0027
OAES	LAT	34.1410	N	0.0280	±	0.0007
OAES	LON	-116.0677	E	0.0259	±	0.0009
OAES	RAD	604.7000	V	0.0007	±	0.0028
BBRY	LAT	34.2643	N	0.0247	±	0.0007
BBRY	LON	-116.8842	E	0.0048	±	0.0009
BBRY	RAD	2051.0515	V	-0.0024	±	0.0029
DSSC	LAT	33.7333	N	0.0241	±	0.0007
DSSC	LON	-116.7121	E	0.0091	±	0.0010
DSSC	RAD	1660.8543	V	0.0011	±	0.0030
PIN1	LAT	33.6122	N	0.0185	±	0.0006
PIN1	LON	-116.4582	E	0.0072	±	0.0007
PIN1	RAD	1256.1866	V	0.0015	±	0.0026
PIN2	LAT	33.6121	N	0.0182	±	0.0006
PIN2	LON	-116.4576	E	0.0072	±	0.0007
PIN2	RAD	1258.3847	V	0.0025	±	0.0026
AZRY	LAT	33.5401	N	0.0165	±	0.0006
AZRY	LON	-116.6297	E	0.0060	±	0.0007
AZRY	RAD	1265.6960	V	0.0019	±	0.0027
ROCH	LAT	33.6110	N	0.0189	±	0.0007
ROCH	LON	-116.6098	E	0.0073	±	0.0007
ROCH	RAD	1393.7155	V	0.0045	±	0.0028
BMRY	LAT	33.9627	N	0.0186	±	0.0007
BMRY	LON	-116.9847	E	0.0106	±	0.0008
BMRY	RAD	787.2481	V	0.0015	±	0.0027
AVRY	LAT	34.4683	N	0.0063	±	0.0007
AVRY	LON	-117.1540	E	-0.0201	±	0.0008
AVRY	RAD	888.9088	V	-0.0052	±	0.0027
CRFP	LAT	34.0391	N	0.0136	±	0.0007
CRFP	LON	-117.0997	E	0.0064	±	0.0008
CRFP	RAD	688.7993	V	0.0006	±	0.0028
PPBF	LAT	33.8357	N	0.0116	±	0.0007
PPBF	LON	-117.1821	E	0.0054	±	0.0009
PPBF	RAD	428.0940	V	0.0022	±	0.0028
COTD	LAT	33.7325	N	0.0216	±	0.0014
COTD	LON	-116.3869	E	0.0054	±	0.0019

COTD	RAD	27.7708	V	0.0164	±	0.0057
PMOB	LAT	33.3572	N	0.0107	±	0.0007
PMOB	LON	-116.8595	E	0.0034	±	0.0010
PMOB	RAD	1662.5250	V	-0.0025	±	0.0030
MLFP	LAT	33.9184	N	0.0082	±	0.0007
MLFP	LON	-117.3180	E	0.0031	±	0.0007
MLFP	RAD	472.9735	V	-0.0019	±	0.0027
MSOB	LAT	34.2308	N	0.0077	±	0.0007
MSOB	LON	-117.2101	E	-0.0033	±	0.0008
MSOB	RAD	1733.1387	V	-0.0012	±	0.0029

The parameters shown are from an inversion of the GPS displacement data using an elastic half-space model. The longitude, latitude and depth of the fault refer to the south-east top corner.

TABLE 2

	8 parameter inversion			6 parameter inversion			
	estimate	formal error	scaled error	estimate	formal error	scaled error	
lat	34.379	0.005	0.01	34.422	0.006	0.014	deg
lon	243.804	0.002	0.004	243.791	0.002	0.004	deg
depth	0.0	fixed	fixed	0.0	fixed	fixed	km
strike	30.0	0.2	0.4	26.4	0.15	0.4	deg NNW
dip	84.2	1.2	2.4	90	fixed	fixed	deg ENE
length	46.2	1.3	2.6	33.3	1.2	2.9	km
width	8.2	0.5	1.0	9.8	0.5	1.2	km
strike-slip	301	18	36	380	19	45	cm
dip-slip	145	18	36	0.0	fixed	fixed	cm E up
χ^2/ν	4.1		1.0	5.7		1.0	

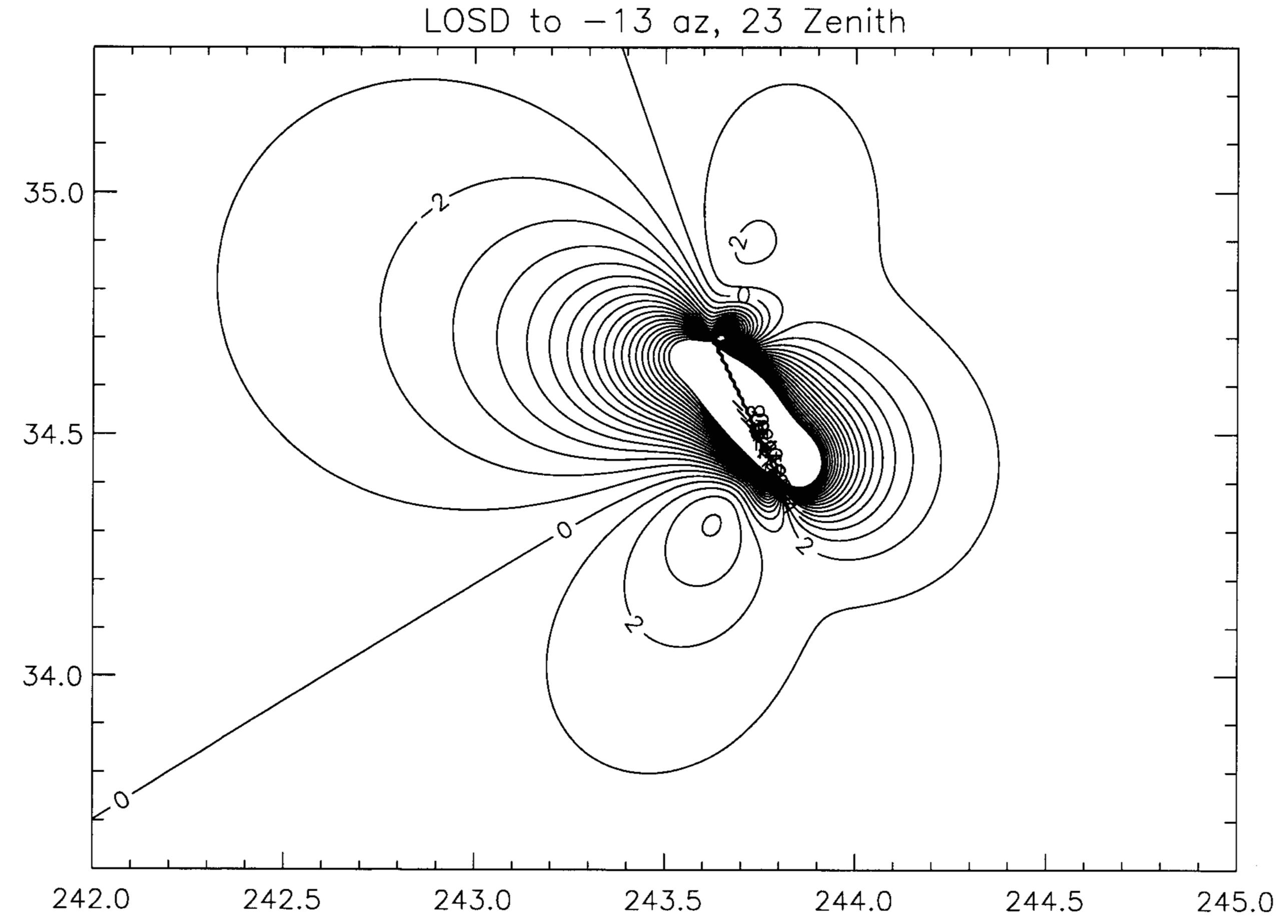
LOSD to −13 az, 23 Zenith
35.0
34.5
34.0
242.0
242.5
243.0
243.5
244.0
244.5
245.0
2
0

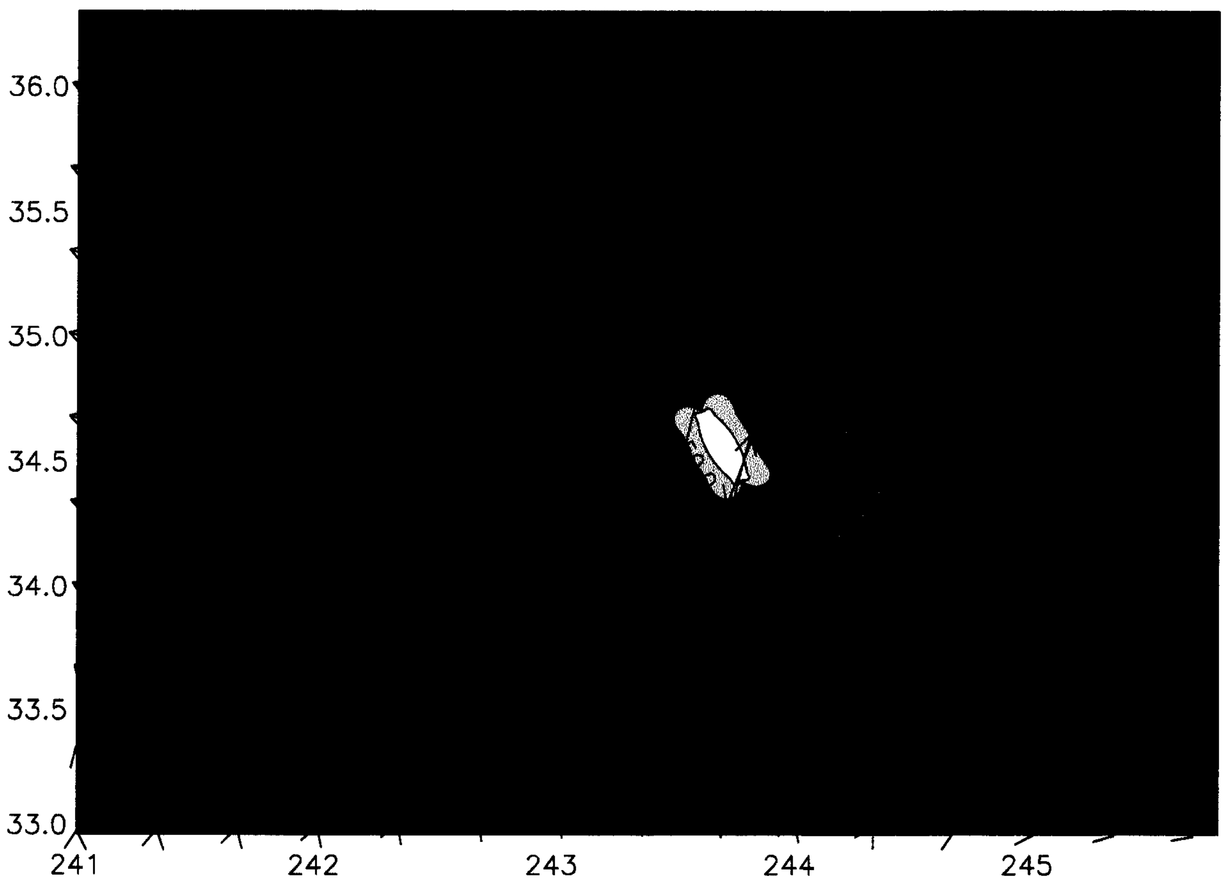
36.0
35.5
35.0
34.5
34.0
33.5
33.0
241
242
243
244
245

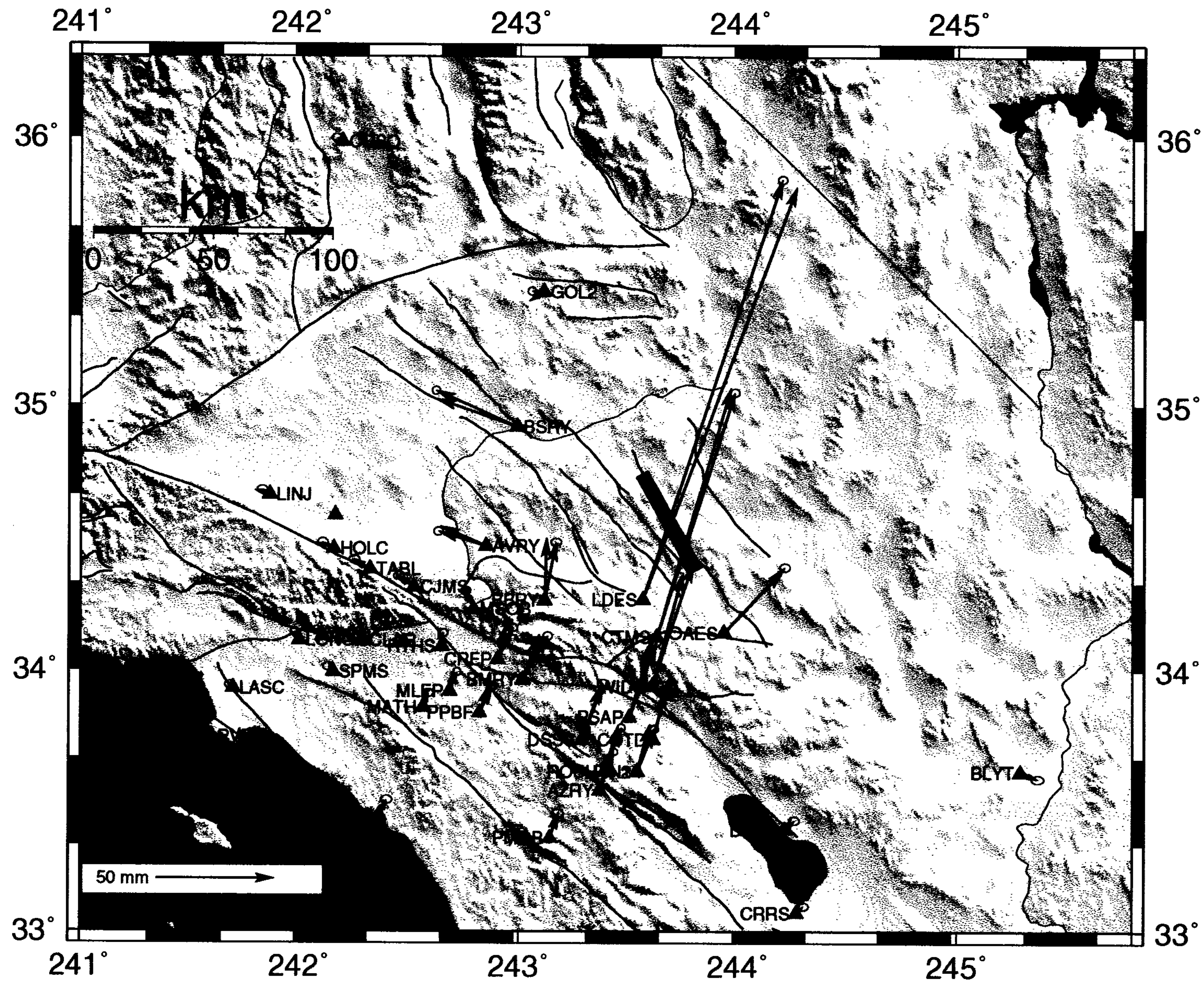

GMT Nov 3 12:16 Figure 1, JPL Hurst 9 day amb fixed - 8 param inversion